Geochemistry Geophysics Geosystems G3

Article
Volume 11, Number 10
1 October 2010
Q10W07, doi:10.1029/2010GC003200
ISSN: 1525-2027

Published by AGU and the Geochemical Society

Upper mantle structure beneath Cameroon from body wave tomography and the origin of the Cameroon Volcanic Line

A. M. Reusch
Department of Geosciences, Pennsylvania State University, University Park, Pennsylvania 16802, USA

Now at Department of Physics, North Carolina Agricultural and Technical State University, Greensboro, North Carolina 27411, USA (angela.reusch@me.com)

A. A. Nyblade
Department of Geosciences, Pennsylvania State University, University Park, Pennsylvania 16802, USA

D. A. Wiens and P. J. Shore
Department of Earth and Planetary Sciences, Washington University, Saint Louis, Missouri 63130, USA

B. Ateba
Branch for Geophysical and Volcanological Research, Institute for Geological and Mining Research, Buea, Cameroon

C. T. Tabod
Department of Physics, University of Yaounde I, PO Box 6052, Yaounde, Cameroon

J. M. Nnange
Institute for Geological and Mining Research, BP 4110, Yaounde, Cameroon

[1] The origin of the Cameroon Volcanic Line (CVL), a 1600 km long linear volcanic chain without age progression that crosses the ocean-continent boundary in west-central Africa, is investigated using body wave tomography. Relative arrival times from teleseismic P and S waves recorded on 32 temporary seismic stations over a 2-year period were obtained using a multichannel cross-correlation technique and then inverted for mantle velocity perturbations. The P and S wave models show a tabular low-velocity anomaly directly beneath the CVL extending to at least 300 km depth, with perturbations of −1.0 to −2.0% for P and −2.0 to −3.0% for S. The S wave velocity variation can be attributed to a 280 K or possibly higher thermal perturbation, if composition and other effects on seismic velocity are negligible. The near vertical sides of the anomaly and its depth extent are not easily explained by models for the origin of the CVL that invoke plumes or decompression melting under reactivated shear zones, but are possibly consistent with a model invoking edge-flow convection along the northern boundary of the Congo Craton lithosphere. If edge-flow convection in the sublithospheric upper mantle is combined with lateral flow channeled along a fracture zone beneath the oceanic sector of the CVL, then the oceanic sector can also be explained by flow in the upper mantle deriving from variations in lithospheric thickness.

Components: 8400 words, 9 figures.

Keywords: intraplate volcanism; upper mantle; mantle convection.

Index Terms: 8121 Tectonophysics: Dynamics: convection currents, and mantle plumes; 7203 Seismology: Body waves; 9305 Geographic Location: Africa.

Received 29 April 2010; **Revised** 8 July 2010; **Accepted** 21 July 2010; **Published** 1 October 2010.

Reusch, A. M., A. A. Nyblade, D. A. Wiens, P. J. Shore, B. Ateba, C. T. Tabod, and J. M. Nnange (2010), Upper mantle structure beneath Cameroon from body wave tomography and the origin of the Cameroon Volcanic Line, *Geochem. Geophys. Geosyst.*, *11*, Q10W07, doi:10.1029/2010GC003200.

Theme: Plate Reconstructions, Mantle Convection, and Tomography Models: A Complementary Vision of Earth's Interior
Guest Editors: D. Müller, S. Quere, and T. Torsvik

1. Introduction

[2] The Cameroon Volcanic Line (CVL) is a ~1600 km long feature traversing both continental Cameroon in West Africa and the offshore islands of Bioko (part of Equatorial Guinea), São Tomé and Príncipe, and Annobón (also part of Equatorial Guinea) (Figure 1a). The CVL is fairly linear, comprised of Eocene to recent alkaline volcanic massifs and Paleocene to Early Oligocene anorogenic plutonic complexes trending ~N30°. Although there are others (e.g., Sala y Gómez, Pukapuka, Austral-Cook [*Koppers et al.*, 2003; *Bonneville et al.*, 2006]), the CVL is one of the best examples of a linear volcanic chain without a clear age progression: Mt. Cameroon in the center of the line is the only active volcano, but volcanism started as early as the Middle Eocene, spreading to almost the entire line during the Late Eocene/Early Oligocene (Figure 1b). All but four of the volcanic centers have been active in the past million years (as evidenced by morphologically recent cinder cones [*Dunlop*, 1983; *Fitton and Dunlop*, 1985]). As ~1000 km of the CVL is continental, it is an excellent area for using an array of land-based seismometers to advance our understanding of how linear volcanic chains without age progression form.

[3] Because the age distribution of the volcanics is not consistent with formation by a single hot spot beneath a moving plate, as suggested by *Morgan* [1983], *Van Houten* [1983], *Lee et al.* [1994], and *Burke* [2001], a number of other models for the origin of the CVL have been proposed. Examples include multiple plumes [*Ngako et al.*, 2006], flow from the Afar plume channeled by thinned lithosphere beneath central Africa [*Ebinger and Sleep*, 1998], decompression melting beneath reactivated shear zones [*Fairhead*, 1988; *Fairhead and Binks*, 1991], and small-scale mantle convection [e.g., *Meyers et al.*, 1998; *King and Anderson*, 1995, 1998; *King and Ritsema*, 2000; *King*, 2007].

[4] To advance our understanding of how the CVL formed, in this study we image variations in the seismic velocity structure of the upper mantle beneath the CVL and surrounding regions. Using broadband seismic data, we determine relative P and S wave arrival time residuals at 32 seismic stations spread across Cameroon from teleseismic events recorded between 2005 and 2007 (Figure 2). We invert the relative arrival time residuals for tomographic images, which reveal strong velocity variations between the upper mantle under the CVL and the regions to the south of the CVL. We then use the images to evaluate several candidate models for the origin of the CVL.

2. Study Area

[5] The Precambrian basement of Cameroon is comprised of the Neoproterozoic Oubanguides mobile belt [*Marzoli et al.*, 2000] and the Archean/Paleoproterozoic Congo Craton [*Cahen et al.*, 1984; *Tchameni et al.*, 2001] (Figure 1a). The location of the western and northeastern boundary of the Congo Craton in southern Cameroon is not well known (Figure 1a). The Oubanguides mobile belt, also known as the North Equatorial Fold Belt [*Toteu et al.*, 2004], is Pan-African in age and formed during the amalgamation of Gondwana [*Nzenti et al.*, 1988].

[6] The Central African Shear Zone (CASZ) lies within the Oubanguides mobile belt and is part of a ENE-WSW Precambrian lineament that stretches many thousand kilometers from the Darfur region of Sudan through the C.A.R. and Cameroon, linking to the Pernambuco fault in Brazil [*Dorbath et al.*, 1986]. In Cameroon, the CASZ is also regionally known as the Ngaoundere [*Wilson and Guiraud*,

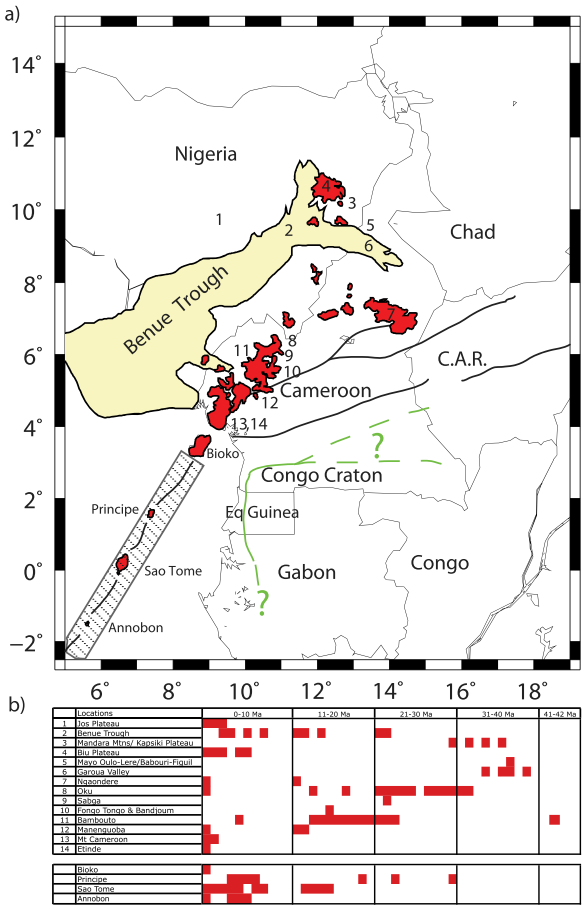

Figure 1. (a) Map of the main geological features of the study region. The volcanics of the Cameroon Volcanic Line are shown in red and the thick black lines trending east-northeast mark the Central African Shear Zone (CASZ) in Cameroon and the Central African Republic. The black numbers show the locations of volcanic localities described in Figure 1b. The stippled region offshore is the inferred location of the Cameroon Fracture Zone [*Sibuet and Mascle*, 1978]. The Benue Trough is shaded in beige and the approximate location of the northern boundary of the Congo Craton is shown by the green line. The location of the Congo Craton boundary to the northeast and west is not well known and possible locations of the boundary are shown with dashed green lines [after *Schlüter*, 2006]. The basement between the Congo Craton and the Benue Trough is comprised of the Oubanguides mobile belt. (b) Chart showing the geographic and temporal extent of Eocene to Recent volcanism in the CVL and Benue Trough. Volcanic localities are listed from northeast to southwest, continental to oceanic. Dates for localities come from *Hedberg* [1969], *Grant et al.* [1972], *Grunau et al.* [1975], *Dunlop and Fitton* [1979], *Cornen and Maury* [1980], *Dunlop* [1983], *Fitton and Dunlop* [1985], *Lee at al.* [1994], *Ngounouno et al.* [1997], *Marzoli et al.* [1999, 2000], *Ngounouno et al.* [2001, 2003], *Njilah et al.* [2004], and *Ngounouno et al.* [2005, 2006].

1992] or Foumbam lineament [*Dorbath et al.*, 1986], before it disappears beneath the Oligocene and younger volcanics at the SW end of the CVL (Figure 1).

[7] To the north of the CVL is the Benue Trough (Figures 1 and 2). Rifting in the Benue Trough started ~140 Ma, coincident with the oldest igneous rocks found there [*Burke*, 1976; *Maluski et al.*, 1995]. It continued to develop during the opening of the equatorial Atlantic (~119–105 Ma [*Fairhead*, 1988]) up until ~84 Ma when it underwent a brief period of compression. Volcanism in the southern Benue Trough continued between 74 and 49 Ma [*Maluski et al.*, 1995].

[8] In Cameroon, alkaline plutonic rocks were emplaced during the period 66–30 Ma in more than 60 separate ring complexes averaging 50–10 km in diameter along the same general trend as the CVL [*Déruelle et al.*, 1991]. Volcanism in the CVL commenced at 42 Ma in the continental sector and at 30 Ma in the oceanic sector (Figure 1b). The earliest volcanism is found on Mt Bambouto, the Mandara Mountains, the Garoua Valley and on the island of Príncipe (Figures 1 and 2). Volcanism continued intermittently along the CVL with most of the volcanic centers experiencing activity within the last 1Ma [*Fitton and Dunlop*, 1985] (Figure 1b). The most recent eruption took place in 2000 at Mt Cameroon.

[9] The volcanic rocks in both the oceanic and continental sectors are dominantly alkaline basalts. They are enriched in radiogenic Sr and Pb and large-ion lithophile elements (LILE) in comparison to mid-ocean ridge basalt (MORB) [*Fitton*, 1985; *Fitton and Dunlop*, 1985; *Halliday et al.*, 1988]. These compositional characteristics have been used to predict a sublithospheric common mantle source to explain the similarity between sectors.

[10] During 1983–1984, the University of Leeds (UK) and ORSTOM (France) deployed short-period vertical-component seismometers in a 300 km long profile across the Adamawa Plateau. Data from the profile were used to calculate P wave travel time residuals and invert for velocity perturbations in the crust and upper mantle. *Dorbath et al.* [1986] found patterns in the residuals uncorrelated to topography, surface geology, or crustal structure. Inversion results showed an ENE-trending low velocity anomaly extending up to 190 km depth beneath the plateau. *Plomerová et al.* [1993] used the same data set with the addition of one more station and a different inversion method to examine lithospheric thickness and anisotropy. They found a 2% low

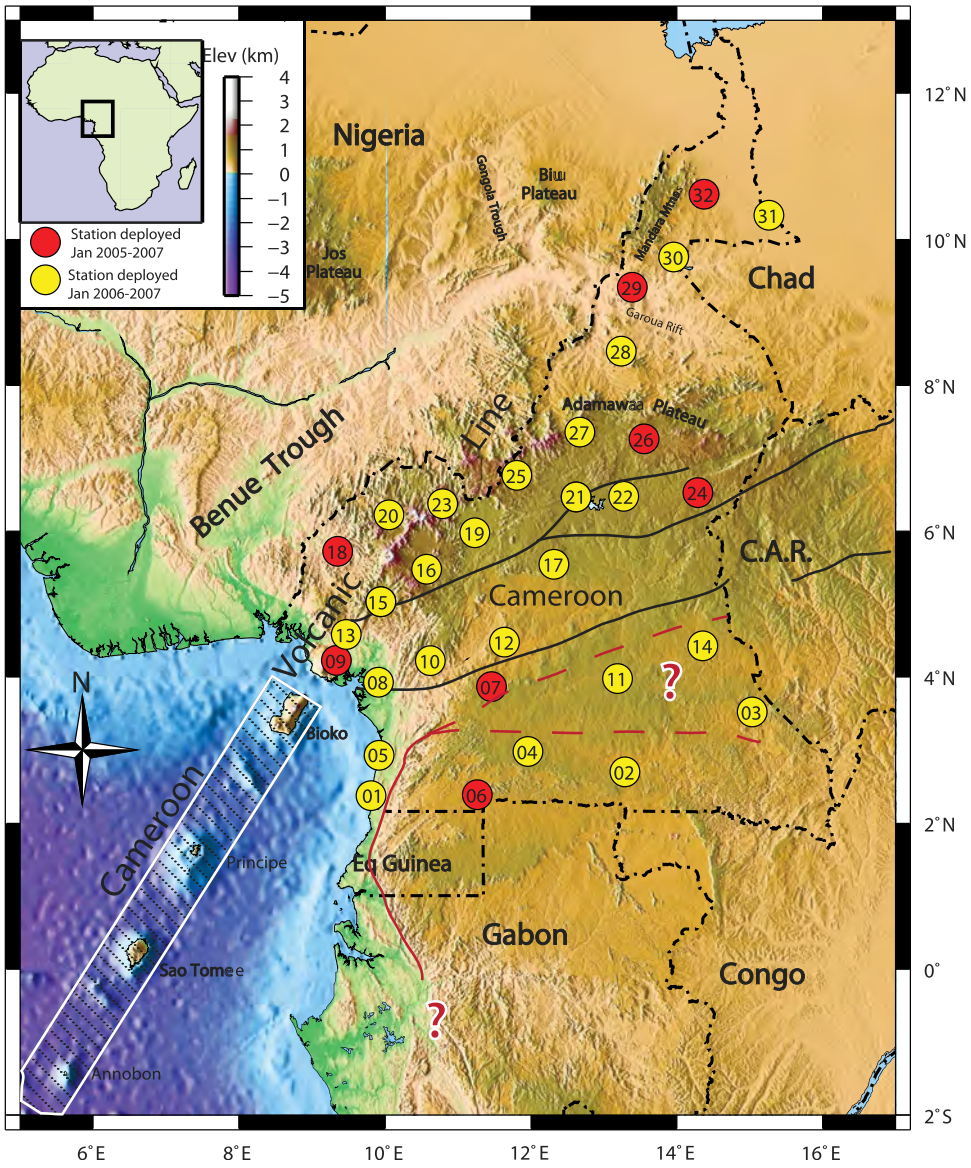

Figure 2. Topographic map showing seismic station locations used for this study. Political boundaries are marked by the dot-dashed line and labeled (C.A.R. = Central African Republic). Major geographic features are also labeled. The circles denote the locations and station numbers of the 32 stations installed across Cameroon for one (yellow circles) or both (red circles) years. The CASZ (solid black lines), Cameroon Fracture Zone (white box), and Congo Craton (red dashed and solid lines) boundary are the same as in Figure 1. The inset map shows the location of the larger map on the continent of Africa.

velocity anomaly in the upper mantle beneath the CASZ and attributed it to asthenosphere welling up in a narrow region.

[11] *Stuart et al.* [1985] used seismic refraction results to demonstrate that the crust is thinned (~23 km thick) north of the Adamawa Plateau beneath the Garoua Rift, compared to an average crustal thickness of 33 km in the southern region of the plateau. More recent seismic studies, using the same data set as this study, suggest that there is little variation in crustal thickness along the CVL. *Tokam et al.* [2010], using a joint inversion of Rayleigh waves and receiver functions to calculate crustal thickness, found Moho depths around 35 km along the CVL. *Tokam et al.* [2010] also suggested that the presence of CVL does not affect the overall structure of the crust in the area when compared to the crustal structure of other Pan African mobile belts. Seismicity studies of the CVL reveal some seismicity (M 0.5–4.0) in the vicinity of Mt Cameroon, the CVL, and extending to the

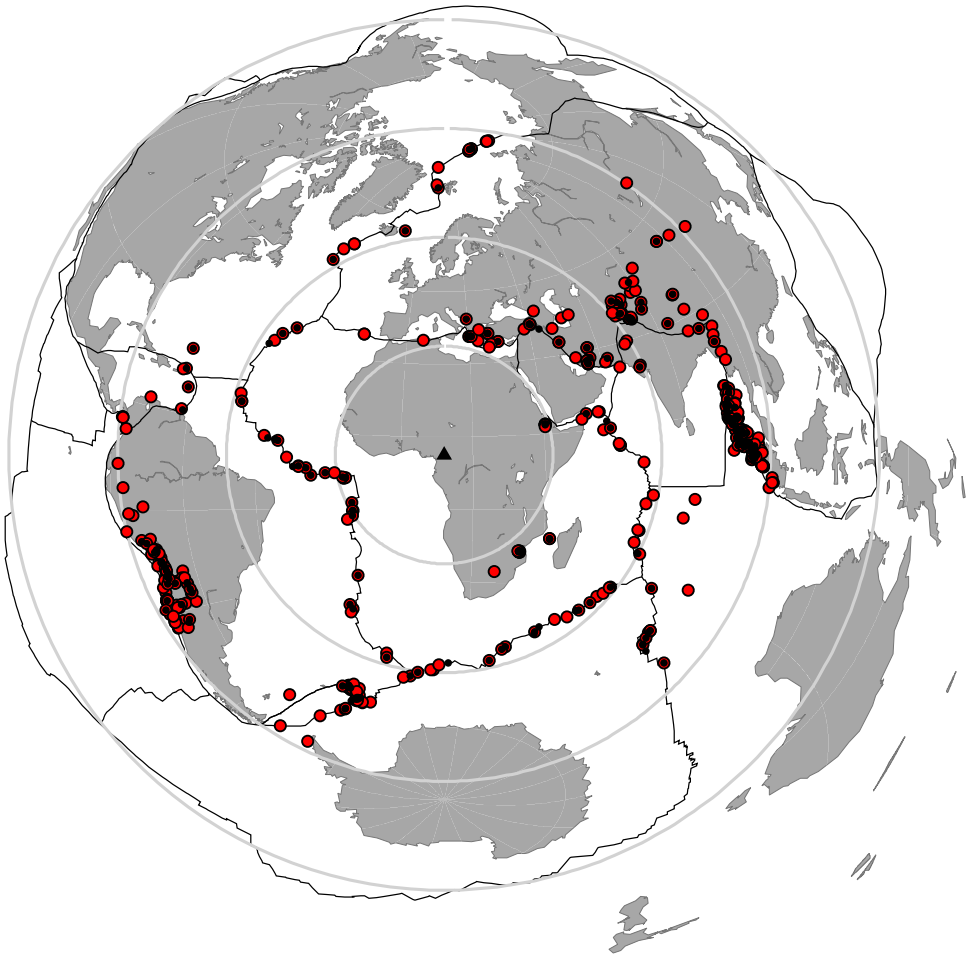

Figure 3. Map of events locations used for P (red circles) and S (black circles) travel times. The black triangle represents the center of the Cameroon array of stations and the concentric circles denote the great circles of angular spacing (in 30° increments) from the center of the experiment.

south, more than halfway toward the border with Equatorial Guinea [*Tabod et al.*, 1992].

[12] Gravity measurements reveal a long wavelength negative Bouguer anomaly (−80 mGal to −120 mGal) associated with the Adamawa Plateau and extending east-southeastward along the CVL [*Djomani et al.*, 1995, 1997; *Nnange et al.*, 2000]. *Djomani et al.* [1995, 1997] utilize spectral analysis of the gravity data to infer that the anomalously hot upper mantle reported by *Dorbath et al.* [1986] is the source of the negative gravity anomaly. They further concluded that the CASZ may be active, providing a conduit through the lithosphere for magma to reach the surface. The study by *Tadjou et al.* [2009] focused on the Proterozoic mobile belt and Congo Craton and reported thick crust (47 km) in the Congo Craton and high gravity gradients between the craton and the Oubanguides mobile belt (e.g., change of −20 to >−100 mGal over distances less than 100 km). *Tadjou et al.* [2009] attribute the high gravity gradient to a major fault zone along the northern boundary of the craton, juxtaposing low-density (~2.67 g/cm^3) Archean crustal rocks to the south against higher density (~2.75 g/cm^3) Proterozoic rocks to the north.

3. Data and Methodology

[13] The data used in this study were recorded between January 2005 and February 2007 by the Cameroon Broadband Seismic Experiment, which consisted of 32 portable broadband seismometers installed across Cameroon (Figure 2). The stations were spaced ~50–150 km apart and were equipped with a broadband seismometer (Guralp CMG-3T and Streckheisen STS-2), a 24bit Reftek digitizer and a GPS clock. Data were recorded continuously at 40 samples per second. Eight stations were

installed in January 2005 and operated for two years; the remaining 24 stations were operated only for the second year of the experiment.

[14] Data from earthquakes with $m_b \geq 5.0$, located at epicentral distances of between 30°–90° for P waves and 30°–84° for S waves and distributed over a wide range of back azimuths were used for this study (Figure 3). The waveforms were filtered using a zero-phase two-pole Butterworth filter with corner frequencies of 0.5–2 Hz for P waves and 0.02–0.2 Hz for S waves, and then the multichannel cross-correlation (MCCC) method of *VanDecar and Crosson* [1990] was used to determine relative arrival times. 6650 P wave relative arrival times were obtained from 643 events and 2713 S wave relative arrival times from 261 events.

[15] For the MCCC, the cross correlation was performed over a 3 s window for the P waves and a 15s window for S waves. In the MCCC method, a relative arrival time residual for each station is calculated and refined using a least squares minimization of the residuals for all station pairs. The mean standard deviation of the relative arrival time residuals is 0.02 s and 0.1 s for P and S waves, respectively. The absolute arrival times for P waves across the network are between ~1 and 3 s later than predicted by the IASP91 model [*Reusch*, 2009].

[16] The relative arrival time residuals were inverted using the method of *VanDecar et al.* [1995]. The model parameterization consisted of 53 knots in latitude between −3.5° and 16°, 42 knots in longitude between 4° and 20°, and 28 knots in depth, extending from the surface to 1000 km depth, for a total of 62,328 knots. The knots were spaced 0.25° apart in both latitude and longitude within the central portion of the model.

[17] The inversion method of *VanDecar et al.* [1995] simultaneously inverts for slowness perturbations, station terms, and event relocations using an iterative procedure (conjugate gradients). Influences on the relative arrival time residuals times from heterogeneous structure outside the model domain are mapped into the event relocations, while the influences arising from crustal and uppermost mantle structure that is poorly imaged because of limited crossing raypaths in the upper ~100 km of the model domain are mapped into the station terms. The IASP91 model [*Kennett and Engdahl*, 1991] was used as the starting model for the inversion. The tradeoff between how well the data are fit and model roughness was explored. The final inversion resulted in a ~95% reduction (the percent difference between the RMS misfit to the data before and after the inversion) of the relative arrival time residuals for both P and S waves. Of this reduction, approximately 10% is accounted for by the station terms and event relocations in both P and S wave models.

4. Results

4.1. P Wave Results

[18] Depth slices through the P wave tomography reveal a low velocity zone (LVZ) of approximately δVp = −1 to −2% (relative to the average velocity in the model space) in the upper mantle beneath the CVL with faster velocities to the southeast of the CVL (Figures 4a–4d). The LVZ also appears to extend under the oceanic sector of the CVL. The change from negative to positive anomalies perpendicular to the strike of the CVL is fairly abrupt, occurring over a distance of ≤100 km. Cross sections along and normal to the strike of the CVL (Figure 4e) show the anomaly extending from perhaps as shallow as 50 km to depths >300 km with near vertical sides. The peak low-velocity amplitude occurs at about 300 km depth. The peak positive amplitude to the southeast of the CVL is >2% at depths between 200 and 300 km.

4.2. P Wave Resolution Tests

[19] To assess model resolution, checkerboard and "tabular body" tests were performed in order to identify how well a known input structure can be resolved. The checkerboard test consisted of an input model of alternating positive and negative (±5%) spherical velocity anomalies with a radius of 50 km in layers at 100, 300, and 500 km depth. A random error of 0.02 s was added to the synthetic relative arrival time residuals generated for the checkerboard model, and then the residuals were inverted using the same smoothing and flattening parameters as were used for the P wave model shown in Figure 4a.

[20] The test reveals that lateral resolution is good within the center of the seismic array, between 3 and 7°N latitude and 10–14°E longitude, with the 50 km radius spheres being well-resolved at 100, 300, and 500 km depths (Figures 5a–5c). As expected from the near-vertical raypath of the P waves, there is some vertical smearing between checkers of the same polarity. The most significant smearing (up to 200 km) occurs in the longitudinal direction (Figure 5d).

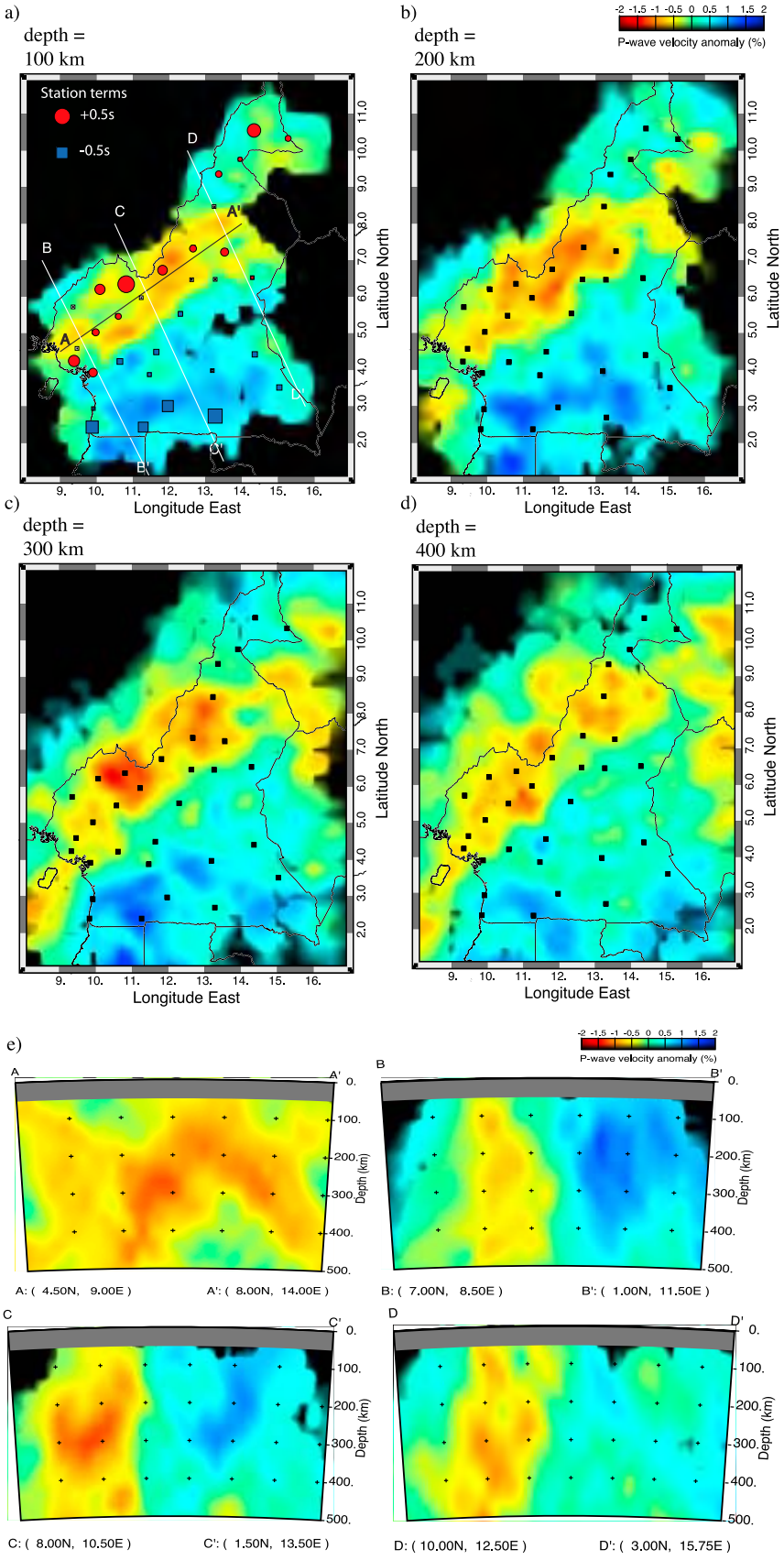
a)
depth =
100 km
Station terms
+0.5s
-0.5s
A
A'
B
B'
C
C'
D
D'
b)
depth =
200 km
P-wave velocity anomaly (%)
-2 -1.5 -1 -0.5 0 0.5 1 1.5 2
c)
depth =
300 km
d)
depth =
400 km
Latitude North
Longitude East
e)
Depth (km)
A: (4.50N, 9.00E)
A': (8.00N, 14.00E)
B: (7.00N, 8.50E)
B': (1.00N, 11.50E)
C: (8.00N, 10.50E)
C': (1.50N, 13.50E)
D: (10.00N, 12.50E)
D': (3.00N, 15.75E)

Figure 4

[21] A resolution test using a tabular body was performed by using a linear, tabular LVZ extending the length of the CVL. The input anomaly is 750 km long and the half-width is 50 km with a Gaussian fall-off to zero. The amplitude of the input anomaly is −5% and the dip of the tabular body is 90°. Figures 6a and 6b show two input models with tabular bodies starting at 100 km depth but with different top-to-bottom thicknesses. Figure 6a shows a 100 km thick tabular body and Figure 6b shows a 200 km thick tabular body. Similar to the checkerboard tests, a synthetic travel time data set was generated and then inverted.

[22] The structures obtained from the inversions are shown in Figures 6c and 6d and can be used to estimate the depth extent of the LVZ. Both input tabular bodies are resolved along their entire length but with the maximum amplitude reduced by 68% for the 100 km thick tabular body and 40% for the 200 km thick tabular body. In both cases, the sides of the recovered anomaly are nearly vertical, similar to the input model. For the 100 km thick input tabular body, the LVZ smears downward about 100 km to a depth of 300 km, but does not reach a depth of 500 km, as seen in the tomographic image (Figure 4e). In comparison, for the 200 km thick input tabular, the recovered anomaly does extend to a depth of about 500 km. The fact that the result for the thicker tabular body more closely matches the result for the real data indicates that the LVZ extends to a depth of at least 300 km (i.e., the depth of the bottom of the 200 km thick input tabular body), and possibly even deeper.

4.3. S Wave Results

[23] Depth slices through the S wave tomography reveal the amplitude of the δVs LVZ to be ~−2 to −3% beneath the CVL, and located in the same region as the P wave anomaly (Figures 7a–7d). Also similar to the P wave results, there is a sharp boundary between the negative velocity anomaly beneath the CVL and the positive anomaly to the south. Cross sections along and normal to the strike of the CVL (Figure 7e) show the anomaly extending to depths > 300 km with near vertical sides, consistent with the P wave anomaly.

4.4. S Wave Resolution Tests

[24] Similar to the P wave resolution tests, the checkerboard tests and "tabular body" tests were performed using the S wave data set. Inputs models were the same as for the P wave resolution tests, but the random error that was added to the synthetic relative travel time residuals was 0.1 s. Results are shown for the S wave checkerboard resolution tests in Figure 4b. Similar to the P wave tests, the best resolution for the S wave checkerboard test is found within the center of the array where the 50 km radius spheres are well resolved at 100, 300, and 500 km depths. The S wave "tabular body" resolution test results contained smearing downward of 100 to 200 km depending on the thickness of the input tabular body, similar to what was found for the P wave tabular body test.

5. Discussion

[25] In this section, we discuss the implications of our tomographic images for geodynamic models that address the origin of the CVL. To summarize, the main feature in our images is a tabular LVZ under the CVL. The P wave anomaly varies in amplitude from −1 to −2%, and the S wave anomaly varies in amplitude from −2 to −3%. Both the P and S models show that the anomaly continues along the length of the CVL and extends to ≥300 km depth. The southeast side of the anomaly is near vertical. The northwest side is not as well imaged as the southeast side but it also appears to be near vertical to depths of ~300 km, and there exists little evidence for any dipping of the anomaly to the northwest under the Benue Trough.

[26] In the upper-mantle, temperature has a stronger influence on seismic velocities than compositional variations [*Goes et al.*, 2000], which are thought to be <1% [*Sobolev et al.*, 1996]. Other factors that can affect seismic velocities are the presence of partial melt or water, and anisotropy [*Sobolev et al.*, 1996; *Goes et al.*, 2000]. Assuming that the LVZ is primarily caused by a thermal anomaly, the temperature perturbation needed to explain the LVZ in the S wave model can be estimated using a temperature derivative of 0.8 m/s/K at an average

Figure 4. Depth slices at (a) 100, (b) 200, (c) 300, and (d) 400 km for the P wave tomography results. The political and coastal boundaries are delineated by the black lines. Station locations are shown by black boxes and in the 100 km depth slice, the red circles and blue squares indicate magnitude and sign of the station terms. White lines on the 100 km depth slice indicate the locations for the cross sections shown in Figure 4e. Areas of the model with a hit count of ≤4 are shaded black. (e) Cross sections for the P wave tomography. Cross section A is a cross-section directly under the CVL and cross sections B-D are normal to the CVL.

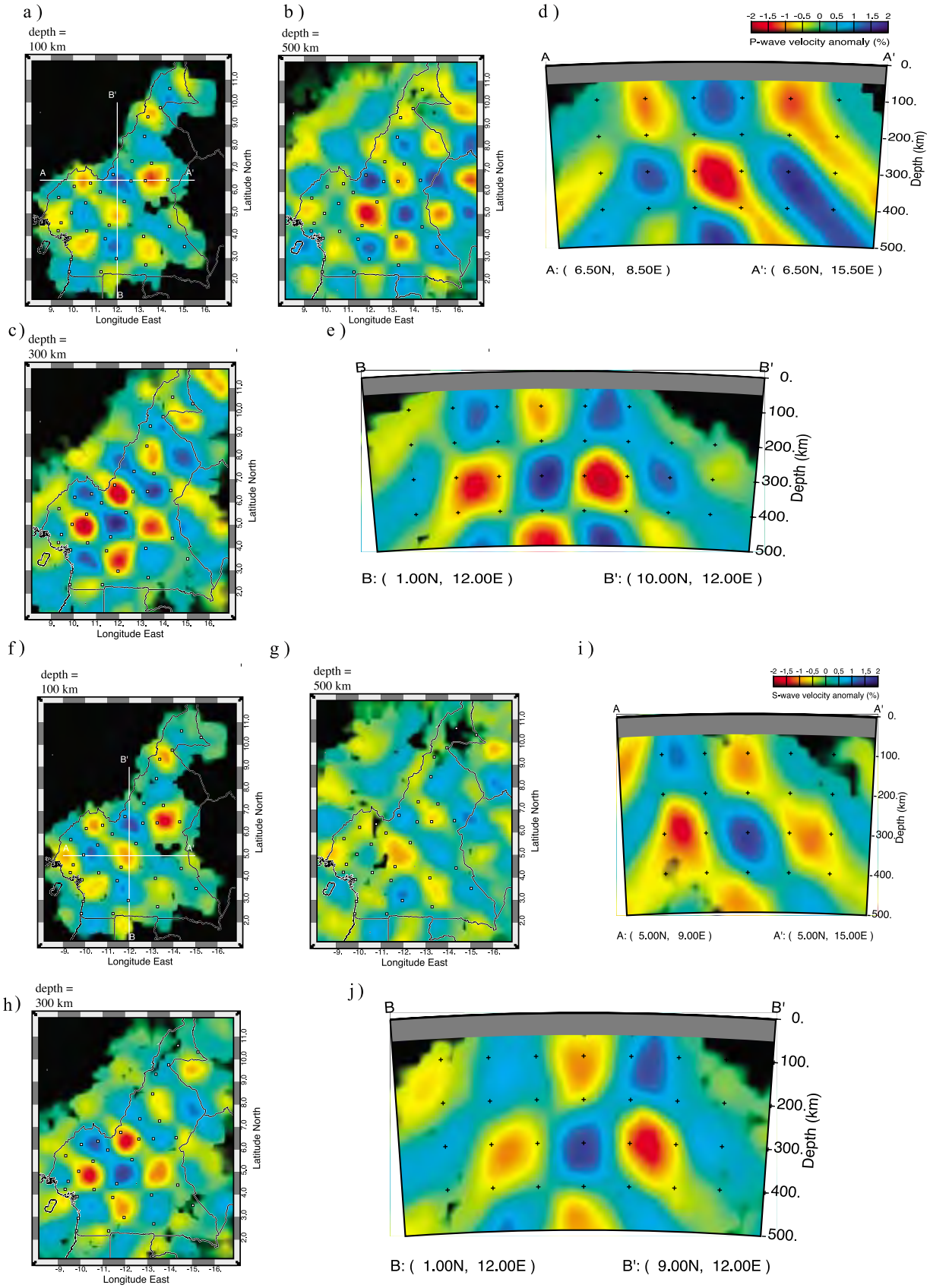
a)
depth = 100 km
b)
depth = 500 km
d)
P-wave velocity anomaly (%)
A: (6.50N, 8.50E)
A': (6.50N, 15.50E)
Depth (km)
c)
depth = 300 km
e)
B: (1.00N, 12.00E)
B': (10.00N, 12.00E)
f)
depth = 100 km
g)
depth = 500 km
i)
S-wave velocity anomaly (%)
A: (5.00N, 9.00E)
A': (5.00N, 15.00E)
h)
depth = 300 km
j)
B: (1.00N, 12.00E)
B': (9.00N, 12.00E)
Latitude North
Longitude East

Figure 5

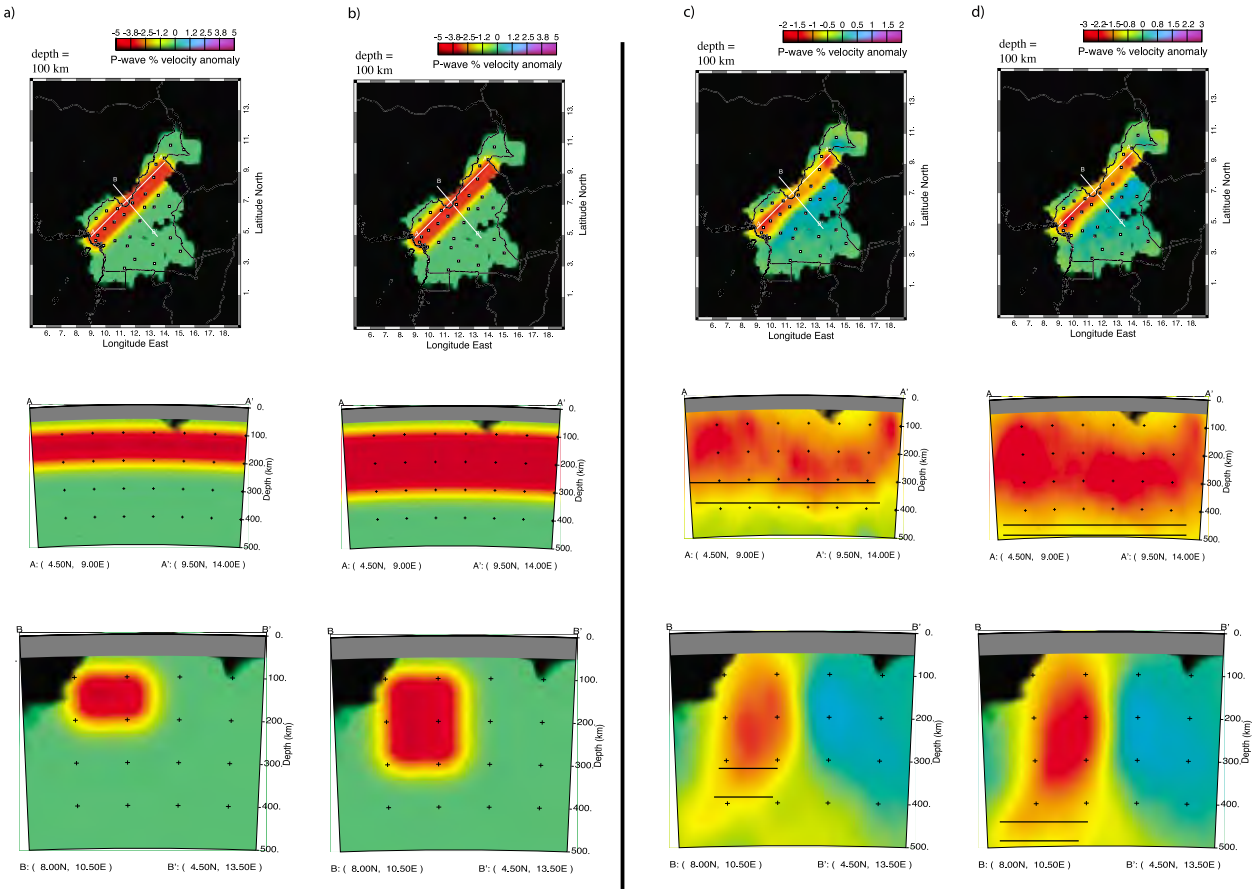

Figure 6. P wave tabular body resolution test input models, showing a tabular body starting at 100 km and extending to (a) 200 km and (b) 300 km depth, beneath the CVL. (c and d) Output models for the P wave tabular body resolution tests. The top black line marks the change below which the amplitudes are less than −1.0% and the bottom black line indicates amplitudes less than −0.5%. Areas of the model with a hit count of ≤4 are shaded black. Note the scale change from Figures 6a and 6b.

temperature of 1300°C for a 10 mm upper mantle grain size at 100 km depth [*Faul and Jackson*, 2005; *Wiens et al.*, 2008]. The peak-to-peak S wave velocity variation is found to be ~5% (Figure 7), yielding a temperature difference of 280 K. The amplitude resolved in the resolution tests suggest that the magnitude of the low-velocity anomaly in the S wave model could be underestimated, and thus the temperature difference could possibly be somewhat higher than 280 K.

[27] Several models have been proposed for the formation of the CVL, generally falling into two groups, plume and non-plume. Shown in Figures 8a and 8b are illustrations of the plume-based models. Non-plume models, shown in Figures 8c–8e, invoke small-scale convection induced by 1) reactivation of the CASZ, 2) temperature differences in the upper mantle, and 3) shearing localized at the base of the mantle transition zone.

[28] *Morgan* [1983], *Van Houten* [1983], *Lee et al.* [1994], and *Burke* [2001] use single plumes to explain the CVL (Figure 8a), noting that its orientation is nearly coincident with the absolute plate motion direction for Nubia over much of the

Figure 5. (a–e) Depth slices and cross sections demonstrating the resolution of the P wave model. Figures 5a–5c are the output from an input model of ±5% alternating 50 km spheres centered at 100, 300, and 500 km depths. Figures 5d and 5e are the cross sections marked in the 100 km depth slice. Areas of the model with a hit count of ≤4 are shaded black. (f–j) Depth slices and cross sections demonstrating the resolution of the S wave model. Figures 5f–5h are the output from an input model of ±5% alternating 50 km spheres centered at 100, 300, and 500 km depths. Figures 5i and 5j are the cross sections marked in the 100 km depth slice. Areas of the model with a hit count of ≤2 are shaded black.

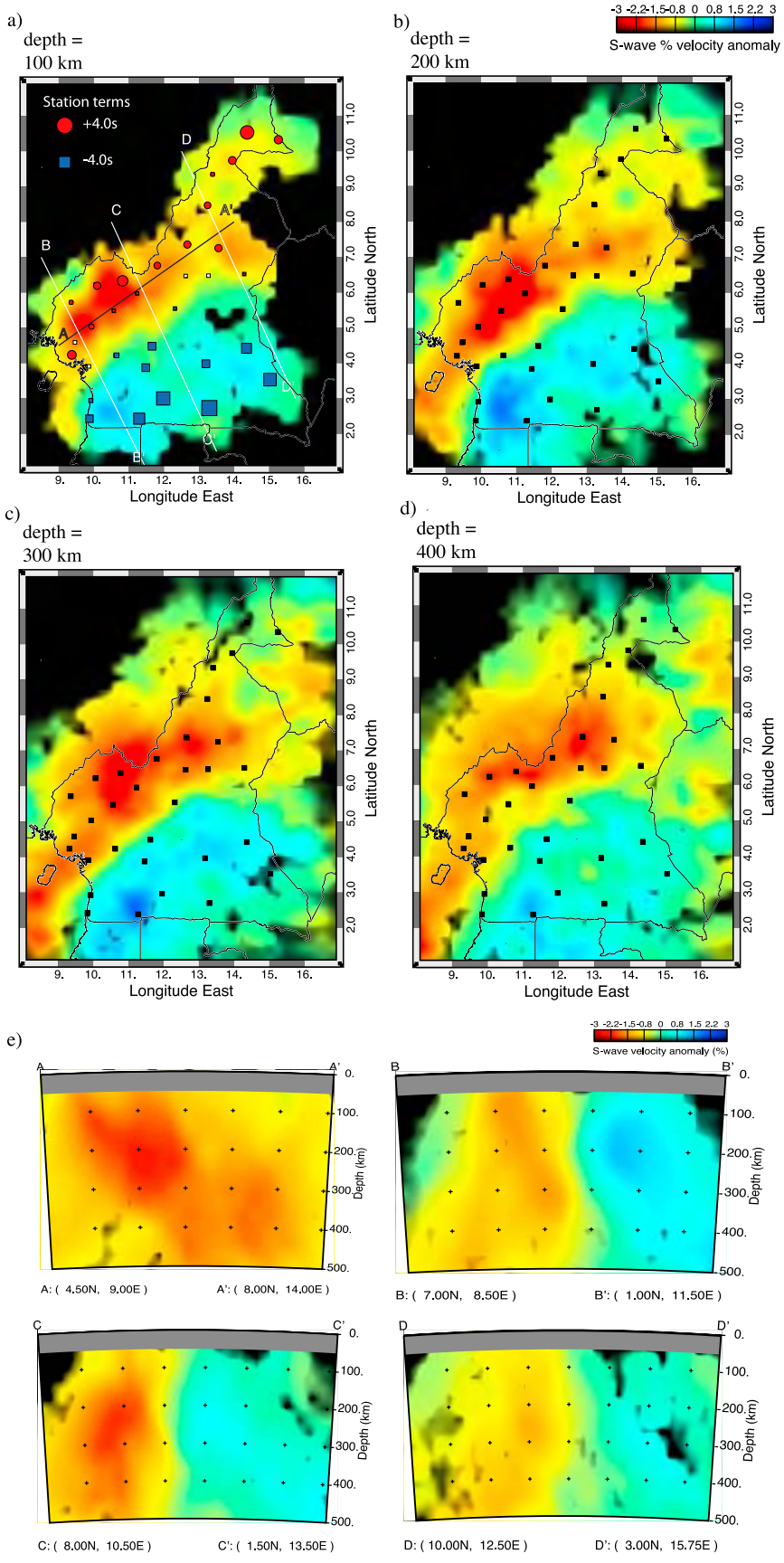
a)
depth =
100 km
Station terms
+4.0s
-4.0s
A
A'
B
B'
C
C'
D
D'
Latitude North
Longitude East
b)
depth =
200 km
-3 -2.2 -1.5 -0.8 0 0.8 1.5 2.2 3
S-wave % velocity anomaly
c)
depth =
300 km
d)
depth =
400 km
e)
S-wave velocity anomaly (%)
Depth (km)
A: (4.50N, 9.00E)
A': (8.00N, 14.00E)
B: (7.00N, 8.50E)
B': (1.00N, 11.50E)
C: (8.00N, 10.50E)
C': (1.50N, 13.50E)
D: (10.00N, 12.50E)
D': (3.00N, 15.75E)

Figure 7

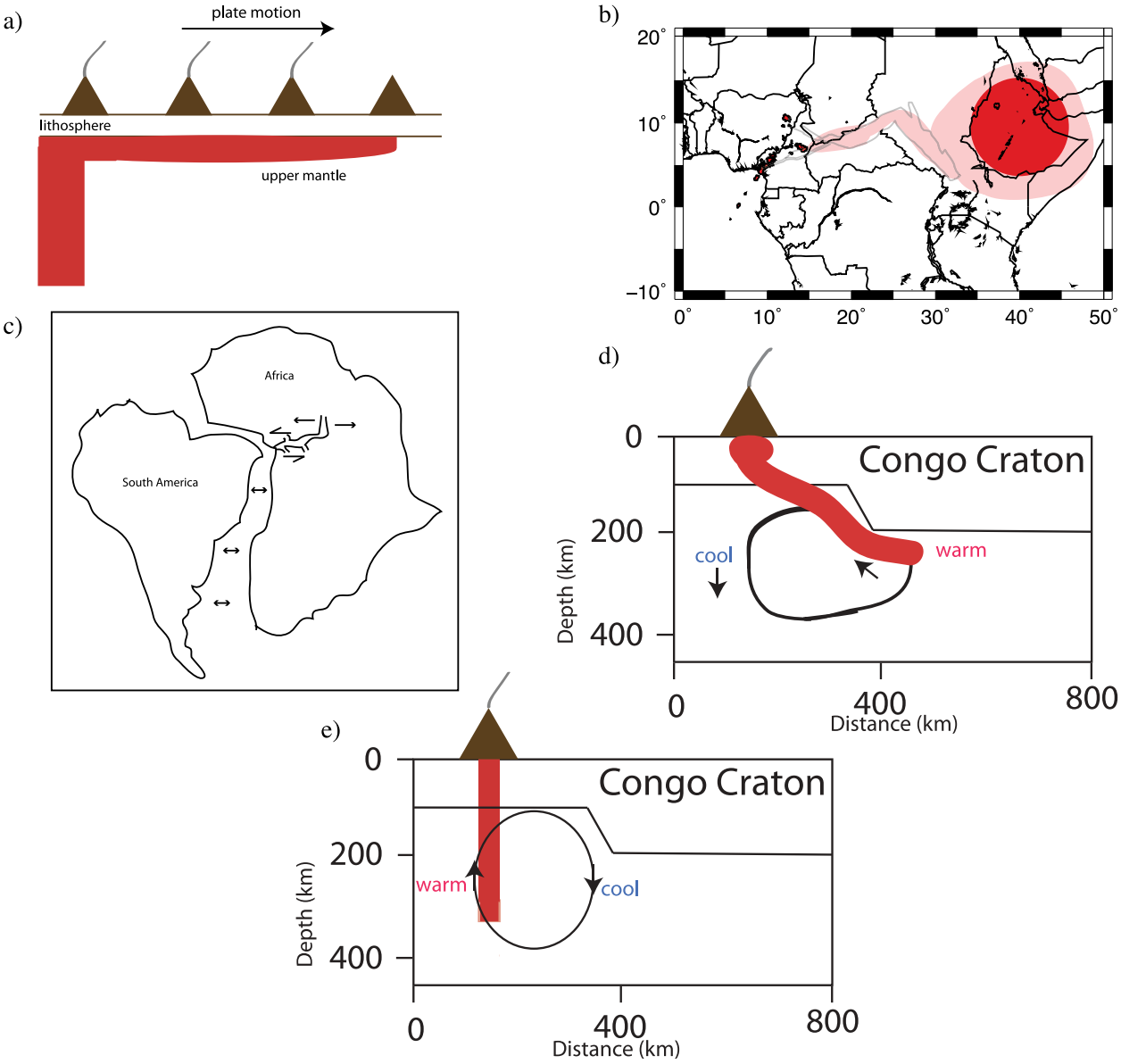

Figure 8. Proposed models for the CVL formation: (a) Single plume, (b) flow from Afar [after *Ebinger and Sleep*, 1998], (c) leaky shear zone [after *Fairhead and Binks*, 1991], (d) edge-flow model one [after *King and Anderson*, 1995], and (e) edge-flow model two [after *King and Ritsema*, 2000].

Cenozoic. However, dating of the volcanic rocks, as reviewed in Figure 1b, shows sporadic volcanism along the entire length of the CVL during the past 42 Ma, which is contrary to what would be expected from a plate moving above a single, stationary plume. To circumvent this criticism, some have suggested that small-scale convection within the plume head might have caused the lack of age progression. For example, *Burke* [2001] postulates that a change in plate motion around 30 Ma generated new upper mantle small-scale (~100 km diameter) convection cells focused in a region of

Figure 7. Depth slices at (a) 100, (b) 200, (c) 300, and (d) 400 km for the S wave tomography results. The political and coastal boundaries are delineated by the black lines. Station locations are shown by black boxes and in the 100 km depth slice, the red circles and blue squares indicate magnitude and sign of the station terms. White lines on the 100 km depth slice indicate the locations for the cross sections shown in Figure 7e. Areas of the model with a hit count of ≤2 are shaded black. (e) Cross sections for the S wave tomography models. Cross section A is a profile directly under the CVL and cross sections B–D are normal to the CVL and demonstrate its vertical-tabular nature.

extension between the nearly right-angle bend in the western edge of the continental margin in Cameroon and the head of the "711" plume located at latitude 7°N, longitude 11.5°E.

[29] In the starting plume model of *Griffths and Campbell* [1990], the plume head flattens against the underside of the lithosphere over an area ~1000–2000 km in diameter, and feeding the plume head is a plume tail ~100–200 km in diameter. When this model is applied to the CVL, the plume head, which would have impinged on the base of the lithosphere no later than ~40 Ma, would no longer be present because of entrainment in mantle convection [*Nyblade and Sleep*, 2003]. But because of the slow movement of the Nubia plate since ~30 Ma, the plume tail could still possibly reside under the CVL and be delivering warm mantle rock to the base of the lithosphere creating a thin (~50–100 km thick) LVZ (Figure 8a) [*Nyblade and Sleep*, 2003]. However, our resolution tests (Figures 6c and 6d) indicate that a minimum depth for the base of the LVZ is 300 km, much deeper than can be attributed to plume material delivered to the base of the lithosphere by a plume tail. Therefore, a model for the origin of the CVL that invokes a plume tail is not favored.

[30] Illustrated in Figure 8b is the *Ebinger and Sleep* [1998] model that shows plume material beneath the CVL coming from the Afar plume. In this model, warmer material travels laterally toward Cameroon from Afar, channeled by regions of thinner lithosphere beneath the Central African Rift System. If the plume impinged on the lithosphere beneath Afar at 45 Ma, then the plume material could have reached the western Adamawa plateau by ~5 Ma [*Ebinger and Sleep*, 1998]. Similar to the plume model discussed above, this model cannot explain the lack of an age progression in the CVL, or the volcanism prior to 5 Ma. The plume material would also result in a low velocity anomaly localized in the upper 100 km of sublithospheric mantle beneath the CVL. As noted above, our tomographic images demonstrate that the low velocity anomaly extends to at least 300 km depth. Therefore, the *Ebinger and Sleep* [1998] model also does not appear to be a viable model for the origin of the CVL.

[31] Another possibility is that the CVL formed from volcanism along a shear zone created during the opening of the Atlantic Ocean. *Fairhead* [1988] and *Fairhead and Binks* [1991] suggest that the opening of the Atlantic reactivated shear zones in the Cameroon/Nigeria area (Figure 8c). The shear zone reactivation was accompanied by lithospheric extension in the interior of the continent related to the differential movement between the opening of the central Atlantic and equatorial Atlantic. This model might explain the sporadic eruption of volcanism along the entire CVL, but the timing of the volcanism predicted by this model is problematic because the Atlantic commenced opening in this region during the Early Cretaceous [*Mascle et al.*, 1986; *Jones*, 1987; *Nzenti et al.*, 1988]. Emplacement of the alkaline ring complexes didn't start until 66 Ma but continued until at least 30Ma [*Déruelle et al.*, 1991] and volcanism only began in the last 42 Ma (Figure 1b). In addition, this model does not account for the low velocity anomaly in our tomographic images extending to at least 300 km depth because the decompression melting would occur just below the lithosphere. Thus, we rule out this model too as a candidate model for the origin of the CVL.

[32] Cameroon is bounded to the south by the Congo Craton and it has been suggested that the difference in lithospheric thickness between the craton and the Proterozoic lithosphere to the north of the craton may have generated edge-driven convection [*King and Anderson*, 1995, 1998; *King and Ritsema*, 2000; *King*, 2007]. *King and Anderson* [1995, 1998] suggest that the insulating effects of the thicker cratonic lithosphere as opposed to thinner "mobile belt" lithosphere result in lithospheric and sublithospheric mantle temperature variations that can lead to two kinds of convective flow regimes (Figures 8d and 8e). In the first case, warmer material from beneath the thick, insulating cratonic lithosphere flows outward toward the thinner lithosphere beneath the mobile belt. The rising material crosses into the melting zone as it reaches the base of the lithosphere beneath the mobile belt. This model predicts that a LVZ would be seen directly beneath the CVL and dip to the southeast with depth toward the Congo Craton (Figure 8d). Such a dipping anomaly is not seen in our tomographic images (Figures 4e and 7e) and so we can also eliminate this edge-flow model as a candidate model for the origin of the CVL.

[33] In the other edge-flow model (Figure 8e), a corner-flow eddy develops due to temperature variations between the cold, cratonic lithosphere and the juxtaposed sublithospheric convecting mantle. The cold lithosphere leads to cooling of the convective mantle rock, inducing a downwelling along the edge of the cratonic lithosphere [*King and Anderson*, 1998; *King and Ritsema*, 2000; *King*, 2007], and a return upwelling develops ~200–

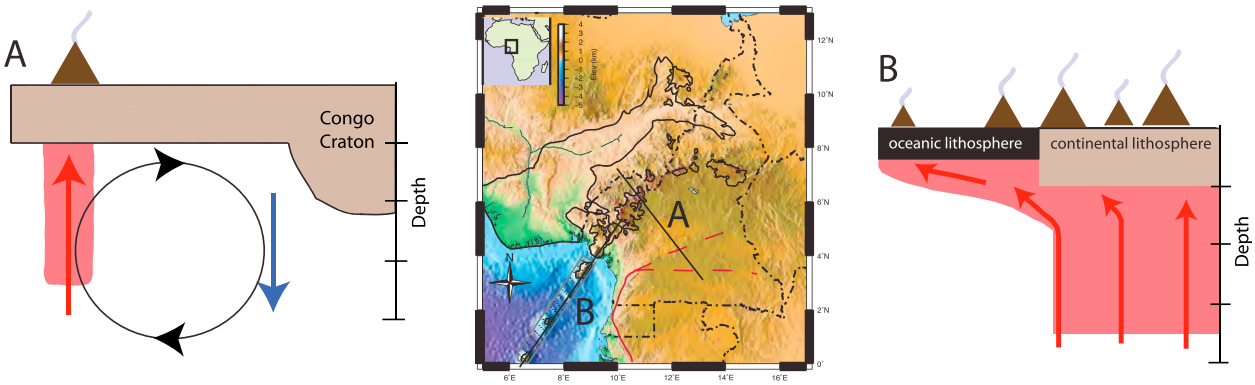

Figure 9. Sketches illustrating our proposed hybrid model for the origin of the CVL. The model invokes edge flow convection (Profile B) and lateral flow (Profile A) beneath the oceanic portion of the CVL channeled by thinner lithosphere under the Cameroon Fracture Zone.

1000 km from the edge of the craton, depending on the scale of convection. The upwelling brings deeper mantle rock to sufficiently shallow mantle depths to generate decompression melting. *King and Ritsema* [2000] show that there is a significant positive velocity anomaly not only beneath the Congo Craton (>350 km depth), but also beneath the mobile belt lithosphere to the north of the craton. They suggest that this positive velocity anomaly beneath the mobile belt is caused by the downwelling in the corner-flow eddy. Our tomographic results are consistent with the *King and Ritsema* [2000] interpretation of edge-driven convection, showing a high velocity anomaly in the upper mantle adjacent to and beneath the Congo Craton (Figures 4 and 7), as well as the LVZ under the CVL.

[34] This model could also explain the homogeneity in bulk geochemical composition of the volcanism in the CVL as reviewed earlier, because a single, sublithospheric mantle source for both the continental and oceanic sections of the CVL could produce compositionally similar volcanics.

[35] A potential problem with this edge-driven convection model, however, is that it does not explain well the linear nature of the CVL. Much of the continental section of the CVL is subparallel to the northern edge of the Congo Craton, and so the linearity of this part of the CVL could possibly be accounted for by the edge-driven convection model. The oceanic part, however, does not parallel the western edge of the Congo Craton (Figures 1 and 2). To explain the linear nature of the oceanic part of the CVL, we offer a "hybrid model" that invokes the upwelling of warm material in the convective eddy being channeled along the presumed location of the Cameroon Fracture Zone (Figures 1a, 2, and 9 [*Sibuet and Mascle*, 1978]), where the lithosphere may be thinner than the surrounding oceanic lithosphere. This mechanism could explain the start and continued feeding of volcanism at the island of Príncipe with a decrease in age of volcanism to the southwestern islands of São Tomé and Annobón.

[36] Another possible issue with the eddy convection model involves the timing of volcanism. Africa and South America were fully separated by 105 Ma, yet the magmatic activity did not begin until 66 Ma and there is no evidence for volcanism prior to 42 Ma. According to *King and Anderson* [1998], the convective eddy will not be fully established until ~50–90 Ma after the initiation of convection. If the edge-flow convection started after the breakup of Africa and South America (~105 Ma), then the initiation of magmatism at 66 Ma can be accounted for. At 30 Ma, the plate motion of the African (Nubian) plate slowed dramatically [*Burke*, 2001], and this slowdown could explain the widespread increase in volcanism around 30 Ma (Figure 1b), because the convective flow regime could have strengthened as the plate slowed down.

6. Summary and Conclusions

[37] In summary, our P and S wave tomographic images show a tabular LVZ extending to at least 300 km depth below the CVL. Our results, when combined with the timing of the volcanism and intrusive magmatism in Cameroon, can be used to argue against all but one of the candidate models for the origin of the CVL. The edge-flow convection model [*King and Anderson*, 1998; *King and Ritsema*, 2000; *King*, 2007] remains a viable model as it could explain the linearity of the onshore

section of the CVL, the timing of volcanism, and the similarities in the geochemical properties of the rocks. And, if it is combined with flow of warmer mantle material channeled along a fracture zone to create the linear offshore part of the CVL, the model can also explain the linearity of the entire volcanic chain.

[38] The full depth extent of the LVZ beneath the CVL is unknown and additional seismic analyses are needed to place tighter constraints on it. Our results indicate that the LVZ extends to at least 300 km, but how much deeper it extends is uncertain. Because the lateral extent of the convection cell in the edge-flow model is proportional to its depth extent [*King and Anderson*, 1998; *King and Ritsema*, 2000; *King*, 2007], and because the CVL volcanics are ~150–400 km from the Congo Craton, the depth extent of the convection cell should be no larger than ~400 km. Thus, understanding the depth to which the LVZ extends is critical for further evaluating the edge-flow model for creating the CVL. For example, a convective cell 600 km deep would lead to an upwelling at ~600 km from the location of the downwelling, which is not consistent with the distance between the CVL and the Congo Craton.

Acknowledgments

[39] We would like to thank Garrett Euler, Alain-Pierre Tokam, Mike Forte, and many other individuals for assistance in with fieldwork, Yongcheol Park and Ian Bastow for help processing the data, and Scott King and two anonymous reviewers for constructive reviews. This work was funded by the National Science Foundation under grants EAR 0310272, EAR 0310094 and OISE 0530062.

References

Bonneville, A., L. Dosso, and A. Hildenbrand (2006), Temporal evolution and geochemical variability of the South Pacific superplume activity, *Earth Planet. Sci. Lett.*, *244*(1–2), 251–269, doi:10.1016/j.epsl.2005.12.037.

Burke, K. (1976), Development of graben associated with initial ruptures of Atlantic Ocean, *Tectonophysics*, *36*(1–3), 93–112, doi:10.1016/0040-1951(76)90009-3.

Burke, K. (2001), Origin of the Cameroon line of volcano-capped swells, *J. Geol.*, *109*(3), 349–362, doi:10.1086/319977.

Cahen, L., N. G. Snelling, G. Delhal, and J. R. Vail (1984), *The Geochronology and Evolution of Africa*, Clarendon, Oxford, U. K.

Cornen, G., and R. C. Maury (1980), Petrology of the volcanic island of Annobón, Gulf of Guinea, *Mar. Geol.*, *36*(3–4), 253–267, doi:10.1016/0025-3227(80)90090-0.

Déruelle, B., C. Moreau, C. Nkoumbou, R. Kambou, J. Lissom, E. Njonfang, R. T. Ghogomu, and A. Nono (1991), The Cameroon Line: A review, in *Magmatism in Extensional Tectonic Structural Settings*, edited by A. B. Kampunzu and R. T. Lubala, pp. 274–327, Springer, Berlin.

Djomani, Y. H. P., J. M. Nnange, M. Diament, C. J. Ebinger, and J. D. Fairhead (1995), Effective elastic thickness and crustal thickness variations in west central Africa inferred from gravity data, *J. Geophys. Res.*, *100*(B11), 22,047–22,070, doi:10.1029/95JB01149.

Djomani, Y. H. P., M. Diament, and M. Wilson (1997), Lithospheric structure across the Adamawa plateau (Cameroon) from gravity studies, *Tectonophysics*, *273*(3–4), 317–327.

Dorbath, C., L. Dorbath, J. D. Fairhead, and G. W. Stuart (1986), A teleseismic delay time study across the Central African Shear Zone in the Adamawa region of Cameroon, West Africa, *Geophys. J. R. Astron. Soc.*, *86*(3), 751–766.

Dunlop, H. M. (1983), Strontium isotope geochemistry and potassium-argon studies on volcanic rocks from the Cameroon Line, West Africa, Ph.D. thesis, Univ. of Edinburgh, Edinburgh, U. K.

Dunlop, H. M., and J. G. Fitton (1979), K-Ar and Sr-isotopic study of the volcanic-Rocks of the island of Príncipe, West Africa—Evidence for mantle heterogeneity beneath the Gulf of Guinea, *Contrib. Mineral. Petrol.*, *71*(2), 125–131, doi:10.1007/BF00375428.

Ebinger, C. J., and N. H. Sleep (1998), Cenozoic magmatism throughout east Africa resulting from impact of a single plume, *Nature*, *395*(6704), 788–791, doi:10.1038/27417.

Fairhead, J. D. (1988), Mesozoic plate tectonic reconstructions of the central South Atlantic Ocean: The role of the West and Central African rift system, *Tectonophysics*, *155*(1–4), 181–191, doi:10.1016/0040-1951(88)90265-X.

Fairhead, J. D., and R. M. Binks (1991), Differential opening of the Central and South Atlantic Oceans and the opening of the West African rift system, *Tectonophysics*, *187*(1–3), 191–203, doi:10.1016/0040-1951(91)90419-S.

Faul, U. H., and I. Jackson (2005), The seismological signature of temperature and grain size variations in the upper mantle, *Earth Planet. Sci. Lett.*, *234*(1–2), 119–134, doi:10.1016/j.epsl.2005.02.008.

Fitton, J. G. (1985), The Cameroon Line West Africa—A comparison between oceanic and continental alkaline volcanism, *J. Geol. Soc.*, *142*, 702.

Fitton, J. G., and H. M. Dunlop (1985), The Cameroon Line, West Africa, and its bearing on the origin of oceanic and continental alkali basalt, *Earth Planet. Sci. Lett.*, *72*(1), 23–38, doi:10.1016/0012-821X(85)90114-1.

Goes, S., R. Govers, and P. Vacher (2000), Shallow mantle temperatures under Europe from P and S wave tomography, *J. Geophys. Res.*, *105*(B5), 11,153–11,169, doi:10.1029/1999JB900300.

Grant, N. K., D. C. Rex, and S. J. Freeth (1972), Potassium-argon ages and strontium isotope ratio measurements from volcanic rocks in northeastern Nigeria, *Contrib. Mineral. Petrol.*, *35*(4), 277–292, doi:10.1007/BF00371310.

Griffths, R. W., and I. H. Campbell (1990), Stirring and structure in mantle starting plumes, *Earth Planet. Sci. Lett.*, *99*(1–2), 66–78, doi:10.1016/0012-821X(90)90071-5.

Grunau, H. R., P. Lehner, M. R. Cleintuar, P. Allenbach, and G. Bakker (1975), New radiometric ages and seismic data from Fuerteventura (Canary Islands), Maio (Cape Verde Islands), and São Tomé (Gulf of Guinea), in *Progress in Geodynamics: Proceedings of the National Symposium on Geodynamics Held in Amsterdam, April 3–4, 1975*, edited by G. J. Borradaile et al., pp. 90–118, North-Holland, New York.

Halliday, A. N., A. P. Dickin, A. E. Fallick, and J. G. Fitton (1988), Mantle dynamics—A Nd, Sr, Pb And O isotopic study of the Cameroon Line Volcanic Chain, *J. Petrol.*, *29*(1), 181–211.

Hedberg, J. D. (1969), A geological analysis of the Cameroon trend, Ph.D. thesis, Princeton Univ., Princeton, N. J.

Jones, E. J. W. (1987), Fracture zones in the equatorial Atlantic and the breakup of western Pangea, *Geology*, *15*(6), 533–536, doi:10.1130/0091-7613(1987)15<533:FZITEA>2.0.CO;2.

Kennett, B. L. N., and E. R. Engdahl (1991), Traveltimes for global earthquake location and phase identification, *Geophys. J. Int.*, *105*(2), 429–465, doi:10.1111/j.1365-246X.1991.tb06724.x.

King, S. D. (2007), Hotspots and edge-driven convection, *Geology*, *35*(3), 223–226, doi:10.1130/G23291A.1.

King, S. D., and D. L. Anderson (1995), An alternative mechanism of flood basalt formation, *Earth Planet. Sci. Lett.*, *136*(3–4), 269–279, doi:10.1016/0012-821X(95)00205-Q.

King, S. D., and D. L. Anderson (1998), Edge-driven convection, *Earth Planet. Sci. Lett.*, *160*(3–4), 289–296, doi:10.1016/S0012-821X(98)00089-2.

King, S. D., and J. Ritsema (2000), African hot spot volcanism: Small-scale convection in the upper mantle beneath cratons, *Science*, *290*(5494), 1137–1140, doi:10.1126/science.290.5494.1137.

Koppers, A. A. P., H. Staudigel, M. S. Pringle, and J. R. Wijbrans (2003), Short-lived and discontinuous intraplate volcanism in the South Pacific: Hot spots or extensional volcanism?, *Geochem. Geophys. Geosyst.*, *4*(10), 1089, doi:10.1029/2003GC000533.

Lee, D.-C., A. N. Halliday, J. G. Fitton, and G. Poli (1994), Isotopic variations with distance and time in the volcanic islands of the Cameroon Line: Evidence for a mantle plume origin, *Earth Planet. Sci. Lett.*, *123*(1–3), 119–138, doi:10.1016/0012-821X(94)90262-3.

Maluski, H., C. Coulon, M. Popoff, and P. Baudin (1995), $^{40}Ar/^{39}Ar$ chronology, petrology and geodynamic setting of Mesozoic to Early Cenozoic magmatism from the Benue Trough, Nigeria, *J. Geol. Soc.*, *152*, 311–326, doi:10.1144/gsjgs.152.2.0311.

Marzoli, A., P. R. Renne, E. M. Piccirillo, C. Francesca, G. Bellieni, A. J. Melfi, J. B. Nyobe, and J. N'ni (1999), Silicic magmas from the continental Cameroon Volcanic Line (Oku, Bambouto and Ngaoundere): ^{40}Ar-^{39}Ar dates, petrology, Sr-Nd-O isotopes and their petrogenetic significance, *Contrib. Mineral. Petrol.*, *135*(2–3), 133–150.

Marzoli, A., E. M. Piccirillo, P. R. Renne, G. Bellieni, M. Iacumin, J. B. Nyobe, and A. T. Tongwa (2000), The Cameroon Volcanic Line revisited: Petrogenesis of continental basaltic magmas from lithospheric and asthenospheric mantle sources, *J. Petrol.*, *41*(1), 87–109, doi:10.1093/petrology/41.1.87.

Mascle, J., M. Marinho, and J. Wannesson (1986), The structure of the Guinean continental margin—Implications for the connection between the Central and the South Atlantic Oceans, *Geol. Rundsch.*, *75*(1), 57–70, doi:10.1007/BF01770178.

Meyers, J. B., B. R. Rosendahl, C. G. A. Harrison, and Z.-D. Ding (1998), Deep-imaging seismic and gravity results from the offshore Cameroon Volcanic Line, and speculation of African hotlines, *Tectonophysics*, *284*(1–2), 31–63, doi:10.1016/S0040-1951(97)00173-X.

Morgan, W. J. (1983), Hotspot tracks and the early rifting of the Atlantic, *Tectonophysics*, *94*(1–4), 123–139.

Ngako, V., E. Njonfang, F. T. Aka, P. Affaton, and J. M. Nnange (2006), The North-South Paleozoic to Quaternary trend of alkaline magmatism from Niger-Nigeria to Cameroon: Complex interaction between hotspots and Precambrian faults, *J. Afr. Earth Sci.*, *45*(3), 241–256, doi:10.1016/j.jafrearsci.2006.03.003.

Ngounouno, I., B. Déruelle, D. Demaiffe, and R. Montigny (1997), New data on the Cenozoic volcanism of the Garoua valley (Upper Benue trough, northern Cameroon), *C. R. Acad. Sci., Ser. II*, *325*(2), 87–94.

Ngounouno, I., C. Moreau, B. Déruelle, D. Demaiffe, and R. Montigny (2001), Petrology of the alkaline undersaturated complex of Kokoumi (Cameroon), *Bull. Soc. Geol. Fr.*, *172*(6), 675–686, doi:10.2113/172.6.675.

Ngounouno, I., B. Déruelle, D. Demaiffe, and R. Montigny (2003), The monchiquites from Tchircotche, Upper Benue valley (northern Cameroon), *C. R. Geosci.*, *335*(3), 289–296, doi:10.1016/S1631-0713(03)00047-6.

Ngounouno, I., B. Déruelle, R. Montigny, and D. Demaiffe (2005), Petrology and geochemistry of monchiquites from Tchircotche (Garoua rift, north Cameroon, Central Africa), *Mineral. Petrol.*, *83*(3–4), 167–190, doi:10.1007/s00710-004-0068-y.

Ngounouno, I., B. Déruelle, R. Montigny, and D. Demaiffe (2006), The camptonites from Mount Cameroon, Cameroon, Africa, *C. R. Geosci.*, *338*(8), 537–544, doi:10.1016/j.crte.2006.03.015.

Njilah, I. K., H. N. Ajonina, K. V. Kamgang, and M. Tchindjang (2004), K-Ar ages, mineralogy, major and trace element geochemistry of the Tertiary-Quaternary lavas from the Ndu Volcanic Ridge N.W. Cameroon, *Afr. J. Sci. Technol.*, *5*(1), 47–56.

Nnange, J. M., V. Ngako, J. D. Fairhead, and C. J. Ebinger (2000), Depths to density discontinuities beneath the Adamawa Plateau region, central Africa, from spectral analyses of new and existing gravity data, *J. Afr. Earth Sci.*, *30*(4), 887–901, doi:10.1016/S0899-5362(00)00058-0.

Nyblade, A. A., and N. H. Sleep (2003), Long lasting epeirogenic uplift from mantle plumes and the origin of the Southern African Plateau, *Geochem. Geophys. Geosyst.*, *4*(12), 1105, doi:10.1029/2003GC000573.

Nzenti, J. P., P. Barbey, J. Macaudiere, and D. Soba (1988), Origin and evolution of the late Precambrian high-grade Yaounde gneisses (Cameroon), *Precambrian Res.*, *38*(2), 91–109, doi:10.1016/0301-9268(88)90086-1.

Plomerová, J., V. Babuska, C. Dorbath, L. Dorbath, and R. J. Lillie (1993), Deep lithospheric structure across the Central African Shear Zone In Cameroon, *Geophys. J. Int.*, *115*(2), 381–390, doi:10.1111/j.1365-246X.1993.tb01193.x.

Reusch, A. M. (2009), Using seismic data to interpret the mechanism for Cenozoic volcanism beneath Ross Island, Antarctica, and the Cameroon Volcanic Line, West Africa, Ph.D. thesis, Pa. State Univ., State College.

Schlüter, T. (2006), *Geological Atlas of Africa: With Notes on Stratigraphy, Tectonics, Economic Geology, Geohazards and Geosites of Each Country*, 1st ed., Springer, New York.

Sibuet, J. C., and J. Mascle (1978), Plate kinematic implications of Atlantic equatorial fracture zone trends, *J. Geophys. Res.*, *83*(B7), 3401–3421, doi:10.1029/JB083iB07p03401.

Sobolev, S. V., H. Zeyen, G. Stoll, F. Werling, R. Altherr, and K. Fuchs (1996), Upper mantle temperatures from teleseismic tomography of French Massif Central including effects of composition, mineral reactions, anharmonicity, anelasticity and partial melt, *Earth Planet. Sci. Lett.*, *139*(1–2), 147–163, doi:10.1016/0012-821X(95)00238-8.

Stuart, G. W., J. D. Fairhead, L. Dorbath, and C. Dorbath (1985), A seismic refraction study of the crustal structure associated with the Adamawa Plateau and the Garoua Rift, Cameroon, West Africa, *Geophys. J. R. Astron. Soc.*, *81*(1), 1–12.

Tabod, C. T., J. D. Fairhead, G. W. Stuart, B. Ateba, and N. Ntepe (1992), Seismicity of the Cameroon volcanic line, 1982–1990, *Tectonophysics*, *212*(3–4), 303–320, doi:10.1016/0040-1951(92)90297-J.

Tadjou, J. M., R. Nouayou, J. Kamguia, H. L. Kande, and E. Manguelle-Dicoum (2009), Gravity analysis of the boundary between the Congo Craton and the Pan-African Belt of Cameroon, *Austrian J. Earth Sci.*, *102*(1), 71–79.

Tchameni, R., K. Mezger, N. E. Nsifa, and A. Pouclet (2001), Crustal origin of Early Proterozoic syenites in the Congo Craton (Ntem Complex), South Cameroon, *Lithos*, *57*(1), 23–42, doi:10.1016/S0024-4937(00)00072-4.

Tokam, A.-P., C. T. Tabod, A. Nyblade, J. Julia, D. A. Wiens, and M. E. Pasyanos (2010), Structure of the crust beneath Cameroon, West Africa, from the joint inversion of Rayleigh wave group velocities and receiver functions, *Geophys. J. Int.*, in press.

Toteu, S. F., J. Penaye, and Y. P. Djomani (2004), Geodynamic evolution of the Pan-African belt in central Africa with special reference to Cameroon, *Can. J. Earth Sci.*, *41*(1), 73–85, doi:10.1139/e03-079.

VanDecar, J. C., and R. S. Crosson (1990), Determination of teleseismic relative phase arrival times using multi-channel cross-correlation and least-squares, *Bull. Seismol. Soc. Am.*, *80*(1), 150–169.

VanDecar, J., D. James, and M. Assumpcao (1995), Seismic evidence for a fossil mantle plume beneath South America and implications for plate driving forces, *Nature*, *378*, 25–31, doi:10.1038/378025a0.

Van Houten, F. B. (1983), Sirte Basin, north-central Libya: Cretaceous rifting above a fixed mantle hotspot, *Geology*, *11*, 115–118, doi:10.1130/0091-7613(1983)11<115:SBNLCR>2.0.CO;2.

Wiens, D. A., J. A. Conder, and U. H. Faul (2008), The seismic structure and dynamics of the mantle wedge, *Annu. Rev. Earth Planet. Sci.*, *36*, 421–455, doi:10.1146/annurev.earth.33.092203.122633.

Wilson, M., and R. Guiraud (1992), Magmatism and rifting in western and central Africa, from Late Jurassic to Recent times, *Tectonophysics*, *213*(1–2), 203–225, doi:10.1016/0040-1951(92)90259-9.